RADIO SCIENCE, VOL. 42, RS3018, doi:10.1029/2006RS003567, 2007



# Modeling and synthesis of circular-sectoral arrays of log-periodic antennas using multilevel fast multipole algorithm and genetic algorithms

Özgür Ergül[1] and Levent Gürel[1,2]

Received 3 October 2006; revised 18 January 2007; accepted 7 February 2007; published 19 June 2007.

[1] Circular-sectoral arrays of log-periodic (LP) antennas are presented for frequency-independent operation and beam-steering capability. Specifically, nonplanar trapezoidal tooth LP antennas are considered in a circular array configuration, where closely spaced antennas occupy a sector of the circle. Electromagnetic interactions of the array elements, each of which is a complicated LP antenna structure, are rigorously computed with the multilevel fast multipole algorithm (MLFMA). Genetic algorithms (GAs) are also employed in combination with MLFMA for synthesis and design purposes. By optimizing the excitations of the array elements via GAs, beam-steering ability is achieved in addition to the broadband (nearly frequency-independent) characteristics of the designed arrays. Computational results are presented to demonstrate the important properties of LP arrays.

**Citation:** Ergül, Ö., and L. Gürel (2007), Modeling and synthesis of circular-sectoral arrays of log-periodic antennas using multilevel fast multipole algorithm and genetic algorithms, *Radio Sci.*, *42*, RS3018, doi:10.1029/2006RS003567.

## 1. Introduction

[2] Log-periodic (LP) antennas have a special importance since they display frequency-independent characteristics over wide ranges of frequency [*DuHamel and Isbell*, 1957; *DuHamel and Ore*, 1958]. It is also desirable to employ these antennas in constructing circular arrays to add beam-steering ability, which can be useful in radar applications. Recently, we investigated full-circular arrays with regularly spaced elements, where the sectors of high directive gain are distributed and are also regularly spaced [*Ergül and Gürel*, 2006]. In that study, genetic algorithms (GAs) were employed in the design procedure to extend the steering ability by increasing the width of the scannable sectors with high directive gain. It was observed that the optimization also suppresses the variations depending on the frequency and improves the frequency independence of the design.

[3] In this paper, we focus on sectoral arrays of the LP antennas, where the elements are placed side by side in a circular arrangement, as depicted in Figure 1. Such an array with closely spaced elements is observed to provide a wider scanning range and higher directive gain compared to the full-circular arrays. Therefore sectoral arrays might be preferable depending on the application. In spite of their advantages, sectoral arrays with closely localized elements do not eliminate the need for the full-circular arrays, where the regularly spaced elements provide narrower but multiple scanning ranges. Therefore we present the arrays in this paper as an alternative configuration for the LP antennas.

[4] We develop an advanced simulation environment based on recent advances in computational electromagnetics to simulate the LP arrays. Electric-field integral equation (EFIE) [*Glisson and Wilton*, 1980] formulation is used to achieve a flexible three-dimensional modeling of the antennas. Fast and reliable iterative solvers, such as the multilevel fast multipole algorithm (MLFMA) [*Song et al.*, 1997], are employed to speed up the design procedures without sacrificing the accuracy. Excitations of the antennas are carefully modeled by the current sources attached to the antennas at the feed locations. GAs are employed for the optimization of the excitations to control the steering of the main beam. We use superposition techniques to improve the efficiency of the optimizations.

[1]Department of Electrical and Electronics Engineering, Bilkent University, Bilkent, Ankara, Turkey.
[2]Computational Electromagnetics Research Center, Bilkent University, Bilkent, Ankara, Turkey.


0048-6604/07/2006RS003567$11.00

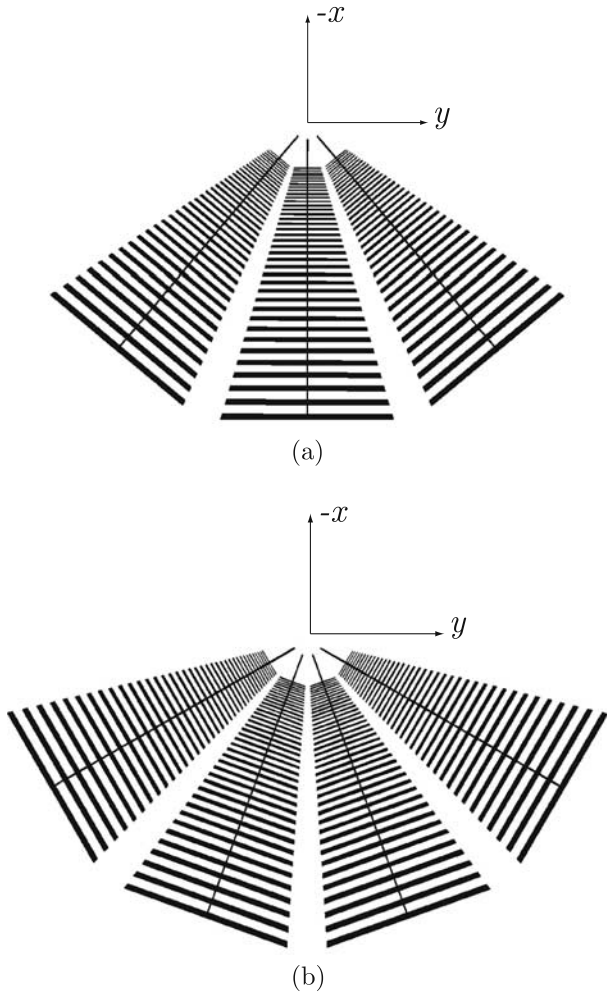


**Figure 1.** Circular-sectoral arrays of closely spaced LP antennas with (a) three elements and (b) four elements.

[5] The rest of the paper is organized as follows. In section 2, we introduce the circular-sectoral arrays of LP antennas. In section 3, we outline the electromagnetic modeling of the LP arrays. Then, in section 4, we discuss the genetic optimization of the excitations for the array elements. In section 5, we present numerical results to demonstrate the beam-steering ability of the designed arrays. Section 6 contains our concluding remarks.

## 2. Circular-Sectoral Arrays of LP Antennas

[6] Figures 1a and 1b present the circular-sectoral arrays of three and four LP antennas, respectively. As the elements of the arrays, we employ the nonplanar trapezoidal tooth LP antenna depicted in Figure 2 and also described by *Ergül and Gürel* [2005], which operates nearly frequency independently in the 300–800 MHz range. Therefore the arrays in Figure 1 are also expected to show broadband characteristics in the same range. However, as demonstrated by *Ergül and Gürel* [2006], frequency independence of the array deteriorates because of the undesired mutual couplings between the antennas, which can be partially remedied by an optimization.

[7] Most of the induced current on an LP antenna exists in a limited area, which is called the active region. The active region is located on the elements that are about a quarter wavelength long [*Stutzman and Thiele*, 1981; *Kraus*, 1988]. Therefore its location depends on the frequency; that is, for low and high frequencies of the operation range, the active region resides on the large and small elements of the antenna, respectively, and partially spills out of the antenna. At intermediate frequencies, for which the active region is completely accommodated on the surface of the antenna, frequency independence is satisfied. In this case, the antenna behaves as if it has an infinite length, since the current out of the active region is negligible. In other words, truncation of the element sequence at both ends of the antenna does not make a difference compared to the theoretical infinite structure [*Rumsey*, 1966; *Mayes*, 1988]. On the other hand, as the active region reaches the ends of the antenna and begins to overflow, the antenna becomes dysfunctional and the frequency independence collapses. Since it is difficult to calculate the size of the active region a priori for a general LP structure, it is also difficult to determine analytically the exact range for the frequency independence. This essential information can be accurately provided by the simulation environment to suggest possible corrections to the design, if necessary [*Ergül and Gürel*, 2005].

[8] For the LP antenna shown in Figure 2, we take the geometric growth factor as $\tau = 0.95$, which means that the two consecutive elements on the antenna are scaled versions of each other with a scale constant of 0.95. Let $f_i$ and $f_{i+1}$ be two distinct frequencies inside the operational range of the antenna with the relation $f_i = \tau f_{i+1}$. The current induced on the antenna at $f_{i+1}$ is approximately the scaled version of the current at $f_i$. This is due to the movement of the active region on the antenna. The scaling factor for the current distribution is also $\tau$, which means that both the frequency and the radiating sources are scaled by the same factor. This ensures that the radiation characteristics of the antenna, such as the pattern and the directive gain, should be the same for $f_i$ and $f_{i+1}$. In general, the radiation characteristics of an LP antenna is not strictly frequency independent, but it is log periodic; that is, it repeats itself at the frequencies scaled by factors of $\tau$.

[9] Variation in the radiation characteristics with respect to the frequency is directly related to the density of the elements on the LP antenna. If $\tau$ is close to unity,

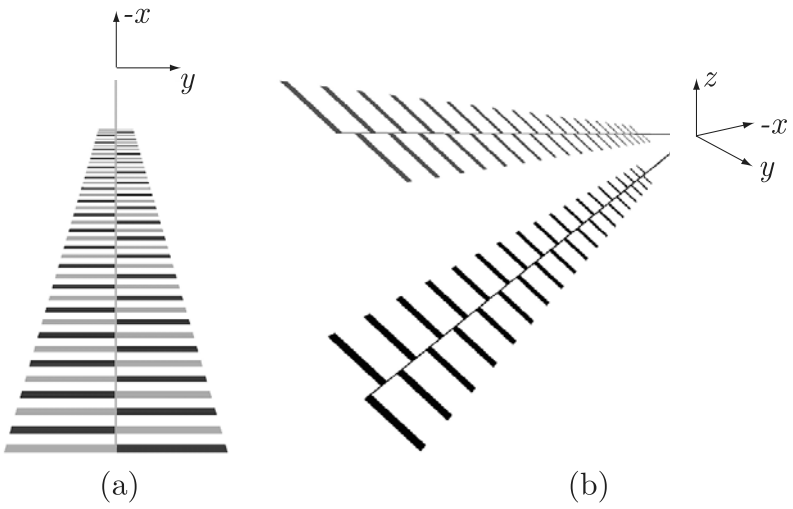


**Figure 2.** Nonplanar trapezoidal tooth LP antenna detailed by *Ergül and Gürel* [2005]: (a) top view and (b) three-dimensional view. This antenna is employed to construct the circular arrays in Figure 1.

which means that the elements are closely spaced, the active region moves on the antenna smoothly. As a consequence, variation in the radiation characteristics becomes small in the interval $[f_i, f_{i+1}]$, where $f_i = \tau f_{i+1}$. On the other hand, for lower values of $\tau$, frequency independence deteriorates because of the large separation between the elements. It should be noted that choosing a small $\tau$ value makes it easier to construct the antenna with fewer elements for the same frequency range of operation. Although this tradeoff between the geometric simplicity and the frequency independence is valid for all LP structures, it becomes increasingly difficult to control the variation in the radiation characteristics as the multiple LP antennas are coalesced in an array configuration. In other words, it might be impossible to obtain the desired level of frequency independence with the highest allowable $\tau$, which is lower than unity because of the nonzero widths of the elements. This is mainly due to the complicated mutual couplings among the antennas, which are impossible to account for analytically and can only be modeled numerically. In order to improve the frequency-independence properties of the LP arrays, we optimize the excitations of the array elements in a highly accurate numerical simulation environment.

## 3. Electromagnetic Modeling

[10] In our simulations, LP antennas and their arrays are modeled with perfectly conducting sheets. The radiation problem is formulated by EFIE derived from the boundary condition for the tangential electric field. Expressing the scattered electric field in terms of the induced surface current $\boldsymbol{J}$, we obtain EFIE in the $\exp(-iwt)$ convention as

$$\hat{\boldsymbol{t}} \cdot \int_{S'} d\boldsymbol{r}' \left[ \overline{\boldsymbol{I}} + \frac{\nabla\nabla}{k^2} \right] g(\boldsymbol{r}, \boldsymbol{r}') \cdot \boldsymbol{J}(\boldsymbol{r}') = \frac{i}{k\eta} \hat{\boldsymbol{t}} \cdot \boldsymbol{E}^{inc}(\boldsymbol{r}), \quad (1)$$

where $\hat{\boldsymbol{t}}$ is any tangential vector at the observation point $\boldsymbol{r}$, $\boldsymbol{E}^{inc}$ is the incident electric field created by the excitations of the antennas, $k$ is the wave number, $\eta$ is the characteristic impedance of the free space, and

$$g(\boldsymbol{r}, \boldsymbol{r}') = \frac{e^{ik|\boldsymbol{r}-\boldsymbol{r}'|}}{4\pi|\boldsymbol{r}-\boldsymbol{r}'|} \quad (2)$$

is the Green's function for the three-dimensional Helmholtz equation.

[11] In order to simultaneously discretize the geometry and EFIE, we expand the unknown surface current in a series of Rao-Wilton-Glisson (RWG) [*Rao et al.*, 1982] basis functions defined on small planar triangles as

$$\boldsymbol{J}(\boldsymbol{r}) = \sum_{n=1}^{N} a_n \boldsymbol{b}_n(\boldsymbol{r}), \quad (3)$$

where $a_n$ is the unknown coefficient of the $n$th basis function and $N$ is the number of unknowns. Projection of EFIE in (1) onto RWG testing functions $\boldsymbol{t}_m$, we obtain the matrix equation

$$\sum_{n=1}^{N} Z_{mn}^{E} a_n = v_m^{E}, \qquad m = 1, .., N, \quad (4)$$

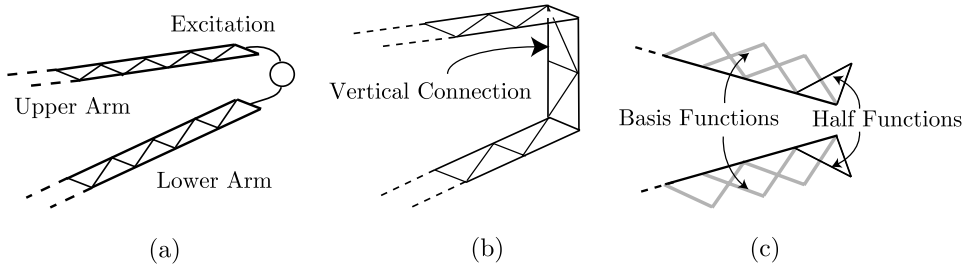


**Figure 3.** (a) Feed location of the LP antenna in Figure 2. (b) Vertical connection to place a delta gap source. (c) Half-basis functions to model a current source without a vertical connection.

where

$$Z_{mn}^{E} = \int_{S_m} d\boldsymbol{r} \boldsymbol{t}_m(\boldsymbol{r}) \cdot \int_{S_n} d\boldsymbol{r}' \left[ \overline{\boldsymbol{I}} + \frac{\nabla\nabla}{k^2} \right] g(\boldsymbol{r}, \boldsymbol{r}') \cdot \boldsymbol{b}_n(\boldsymbol{r}') \tag{5}$$

represents the matrix element, and

$$v_m^{E} = \frac{i}{k\eta} \int_{S_m} d\boldsymbol{r} \boldsymbol{t}_m(\boldsymbol{r}) \cdot \boldsymbol{E}^{inc}(\boldsymbol{r}) \tag{6}$$

represents the $m$th element of the excitation vector. In (5) and (6), $S_m$ and $S_n$ symbolize the spatial supports of the $m$th testing and $n$th basis functions, respectively.

[12] Iterative solution of the $N \times N$ matrix equation in (4) gives the coefficients for the expansion in (3). We then calculate the radiation intensity of the antenna as

$$f(\theta, \phi) = \frac{k^2 \eta^2}{4\pi} \left| \hat{\boldsymbol{\theta}}\hat{\boldsymbol{\theta}} \cdot \boldsymbol{F}(\theta, \phi) + \hat{\boldsymbol{\phi}}\hat{\boldsymbol{\phi}} \cdot \boldsymbol{F}(\theta, \phi) \right|^2, \tag{7}$$

where

$$\begin{aligned} \boldsymbol{F}(\theta, \phi) &= \int_S d\boldsymbol{r} \boldsymbol{J}(\boldsymbol{r}) \exp(-i\boldsymbol{k} \cdot \boldsymbol{r}) \\ &= \int_S d\boldsymbol{r} \sum_{n=1}^{N} a_n \boldsymbol{b}_n(\boldsymbol{r}) \exp(-i\boldsymbol{k} \cdot \boldsymbol{r}) \\ &= \sum_{n=1}^{N} a_n \int_{S_n} d\boldsymbol{r} \boldsymbol{b}_n(\boldsymbol{r}) \exp(-i\boldsymbol{k} \cdot \boldsymbol{r}) \end{aligned} \tag{8}$$

represents the vector current moment and

$$\boldsymbol{k} = k(\hat{\boldsymbol{x}} \sin\theta \cos\phi + \hat{\boldsymbol{y}} \sin\theta \sin\phi + \hat{\boldsymbol{z}} \cos\theta). \tag{9}$$

[13] We need proper representations for the excitations of the antennas in order to achieve accurate modeling of the LP antennas and their arrays. Figure 3a shows the feed location, where the two arms of the LP antenna meet. *Ergül and Gürel* [2005] connected the two arms with a vertical strip as depicted in Figure 3b. Then, we modeled the excitation by employing a delta gap source between a pair of triangles located on the connection. As detailed by *Ergül and Gürel* [2005], the evaluation of the right-hand-side (RHS) excitation vector in (6) for the delta gap source gives

$$v_m^{E} = \left\{ \begin{array}{ll} \pm I_e \dfrac{il_e}{k\eta} & m = e \\ 0 & \text{otherwise} \end{array} \right\}, \tag{10}$$

where $l_e$ is the length of the edge $e$, at which the delta gap source is defined, and $I_e$ is a complex coefficient related to the strength of the feed. For example, if the antenna in Figure 2 is excited by a delta gap source, the RHS vector in (6) will be filled with zeros except for a single nonzero element.

[14] In the present work, instead of the delta gap source, we use another excitation model involving a current source connected to the two arms of the antenna [*Eleftheriades and Mosig*, 1996]. This model does not require an extra vertical conducting strip, on which the delta gap excitation is to be placed. Instead, a current source and a current sink are defined at the tips of the two opposite arms of the antenna to establish the connection electrically. The combination of the source and the sink simulates a current source feeding the antenna. Figure 3c illustrates this model, where we define two half basis functions located at the ends of the arms. Consequently, the matrix equation becomes

$$\sum_{n=1}^{N+2} Z_{mn}^{E} a_n = v_m^{E} = 0, \qquad m = 1, .., N, \tag{11}$$

where the dimension of the equation is increased to $N \times (N + 2)$ because of the extra half functions. In (11), we note that $v_m^{E} = 0$ since there is no incident-field excitation in this case and the integral for the RHS in (6) evaluates

to zero. Assume that the indices of the half basis functions are $e_1$ and $e_2$, where $1 \leq e_1, e_2 \leq N+2$ and $e_1 \neq e_2$. Then, we desire to have

$$a_{e_1} = I_e \tag{12}$$

and

$$a_{e_2} = -I_e \tag{13}$$

in (11), where $I_e$ is a complex coefficient related to the strength of the feed. In other words, the expansion coefficients $a_{e1}$ and $a_{e2}$ are forced to be $\pm I_e$ to simulate the source and the sink. By setting the two coefficients as above, we solve the system

$$\sum_{\substack{n=1 \\ n\neq e_1,e_2}}^{N+2} Z^E_{mn} a_n = -I_e Z_{me_1} + I_e Z_{me_2}, \qquad m = 1,..,N \tag{14}$$

to determine the coefficients $a_n$ for $n \neq e_1, e_2$.

[15] For implementing of the current source, the interactions related to the half basis functions can be evaluated as

$$\begin{aligned} Z^E_{me} &= \int_{S_m} d\boldsymbol{r} \boldsymbol{t}_m(\boldsymbol{r}) \cdot \int_{S_e} d\boldsymbol{r}' \left[\bar{\boldsymbol{I}} + \frac{\nabla\nabla}{k^2}\right] g(\boldsymbol{r},\boldsymbol{r}') \cdot \boldsymbol{b}_e(\boldsymbol{r}') \\ &= \int_{S_m} d\boldsymbol{r} \boldsymbol{t}_m(\boldsymbol{r}) \cdot \int_{S_e} d\boldsymbol{r}' g(\boldsymbol{r},\boldsymbol{r}') \cdot \boldsymbol{b}_e(\boldsymbol{r}') \\ &\quad + \frac{1}{k^2} \int_{S_m} d\boldsymbol{r} \boldsymbol{t}_m(\boldsymbol{r}) \cdot \int_{S_e} d\boldsymbol{r}' \nabla\nabla g(\boldsymbol{r},\boldsymbol{r}') \cdot \boldsymbol{b}_e(\boldsymbol{r}') \\ &= \int_{S_m} d\boldsymbol{r} \boldsymbol{t}_m(\boldsymbol{r}) \cdot \int_{S_e} d\boldsymbol{r}' g(\boldsymbol{r},\boldsymbol{r}') \cdot \boldsymbol{b}_e(\boldsymbol{r}') \\ &\quad + \frac{1}{k^2} \int_{S_m} d\boldsymbol{r} \nabla \cdot \boldsymbol{t}_m(\boldsymbol{r}) \int_{S_e} d\boldsymbol{r}' \nabla g(\boldsymbol{r},\boldsymbol{r}') \cdot \boldsymbol{b}_e(\boldsymbol{r}') \\ &= Z^{E,1}_{me} + Z^{E,2}_{me}, \end{aligned} \tag{15}$$

where $e = e_1$ and $e_2$, and $\boldsymbol{t}_m$ represents divergence-conforming RWG testing functions defined on pairs of triangles. In (15), the value of the inner integral of $Z^{E,2}_{me}$ is singular when the observation point approaches the edge, on which the half RWG basis function $\boldsymbol{b}_e$ is defined. This is more evident when $Z^{E,2}_{me}$ is rewritten as

$$\begin{aligned} Z^{E,2}_{me} &= \frac{1}{k^2} \int_{S_m} d\boldsymbol{r} \nabla \cdot \boldsymbol{t}_m(\boldsymbol{r}) \oint_{\partial S_e} d\boldsymbol{r}' g(\boldsymbol{r},\boldsymbol{r}') \hat{\boldsymbol{u}} \cdot \boldsymbol{b}_e(\boldsymbol{r}') \\ &\quad - \frac{1}{k^2} \int_{S_m} d\boldsymbol{r} \nabla \cdot \boldsymbol{t}_m(\boldsymbol{r}) \int_{S_e} d\boldsymbol{r}' g(\boldsymbol{r},\boldsymbol{r}') \nabla' \cdot \boldsymbol{b}_e(\boldsymbol{r}'), \end{aligned} \tag{16}$$

where the first term involves a line integral around the basis triangle. Since $\hat{\boldsymbol{u}}$ is the normal direction perpendicular to the edges of the basis triangle, the line integral evaluates to zero except for the edge, on which the basis function is defined. On this edge, $\hat{\boldsymbol{u}} \cdot \boldsymbol{b}_e(\boldsymbol{r}') = 1$ and the line integral becomes singular when the observation point approaches to this edge. This singularity is logarithmic and similar expressions are extensively investigated in the context of the magnetic-field integral equation, where we extract the singularity in the outer integral when the testing and basis triangles are touching [*Gürel and Ergül*, 2005]. Then, the integral over the testing triangle can be divided into analytical and numerical parts that can be evaluated separately and accurately. On the other hand, since the logarithmic singularity is quite mild, $Z^{E,2}_{me}$ can be computed to the desired accuracy even for the self interaction of the triangle without resorting to the extraction of the singularity for the outer integrals. This is achieved by sampling the integral inside the triangle with sufficiently high number of integration points without approaching the singular edge.

## 4. Genetic Optimization

[16] GAs have been successfully employed in many computational electromagnetics applications [*Rahmat-Samii and Michielssen*, 1999; *Man et al.*, 1999]. They are especially useful when the optimization space is large and it is difficult to derive an analytical expression for the cost function of the optimization. We therefore employ GAs in this work as described in Figure 4, where a three-element array is shown as an example, to add beam-steering ability to LP arrays. The same procedure is also applied to more populous arrays, where only the number of the optimization variables is changed. Since it is desired to point the main beam in a specific direction, choosing the directive gain as the cost function of the optimization is logical. The directive gain is defined as

$$D(\theta,\phi) = 4\pi \frac{f(\theta,\phi)}{P}, \tag{17}$$

as a function of spherical coordinates ($\theta$, $\phi$), where

$$P = \int_0^{2\pi} \int_0^{\pi} f(\theta,\phi) \sin\theta d\theta d\phi \tag{18}$$

and $f(\theta, \phi)$ represents the radiation intensity derived in (7). We employed GAs to optimize the excitations of the array elements that maximize the directive gain in (17).

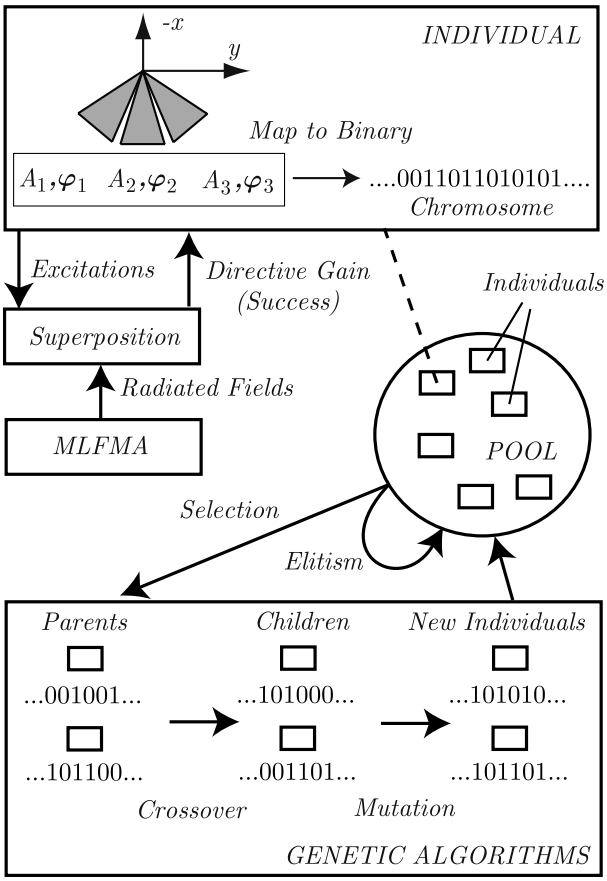


**Figure 4.** Optimization mechanism for the LP arrays involving the genetic algorithms interacting with MLFMA.

Such an optimization of the directive gain in some given ($\theta$, $\phi$) provides the steering of the main beam toward that direction.

[17] GAs work on a pool of individuals (citizens), each of which represents a trial combination of the optimization variables. As depicted in Figure 4, an individual suggests values for the excitations $I_1 = A_1 \exp \varphi_1$, $I_2 = A_2 \exp \varphi_2$, and $I_3 = A_3 \exp \varphi_3$, where $A_{1,2,3}$ and $\varphi_{1,2,3}$ represent the amplitude and the phase, respectively. Without loss of generality, we take $\varphi_3 = 0$ and there are five variables to be optimized for a three-element array. The values of the parameters are selected from the optimization space formed by sampling the variables $A_{1,2,3}$ and $\varphi_{1,2}$ in the [0, 1] and [0°, 360°] ranges, respectively. We observe that uniform samplings with intervals of 0.1 in amplitude and 36° in phase are sufficient, leading to 10 samples for each variable.

[18] We employ a one-to-one map to convert the values represented by each individual into a single lengthy word of binary numbers, called the chromosome. Each individual also has a degree of success, which is simply the value of the cost function of the optimization, i.e., the directive gain at the optimization angle. We define the successful individual as the set of excitations $I_1$, $I_2$, and $I_3$, which results in high directive gain. In the beginning of the optimization, the individuals are created randomly. The optimization is then continued as new generations are formed and the pool is modified progressively. There are three important operations to produce a new generation from the old one:

[19] 1. Crossover: Two successful individuals are selected to exchange some bits of their chromosomes randomly and generate two new individuals called the children. There are various crossover schemes to perform the exchanges [*Rahmat-Samii and Michielssen*, 1999].

[20] 2. Mutation: Some of the binary numbers in the chromosomes are modified randomly; that is, 1 changes into 0 and 0 changes into 1.

[21] 3. Elitism: One or two most successful individuals are preserved in the pool without any modification.

[22] Heuristically, as the new generations are produced and the pool evolves, the overall success of the population increases. In the extreme case, all the individuals are the same with the highest possible success after a number of generations. Then, the optimization is completed and any individual gives the optimal values via an inverse mapping from the chromosome to the excitations. However, it usually is sufficient to interrupt the iterations after a number of generations and select the most successful individual in the pool as the optimization result.

[23] Prior to performing an optimization for an LP array, we carefully adjust the parameters of the GAs by examining the results obtained at some frequencies. We especially consider different values for the parameters, i.e., the size of the pool, the mutation rate, and the number of generations. By checking the final results and convergence characteristics of the GAs, the parameters are selected and fixed so that the same set of parameters is used for all computations at different frequencies. For the optimizations of the LP arrays, we generally use pools with 20–30 individuals and keep the mutation rate for each digit of the chromosomes at about 5%. We apply elitism only for the most successful individual. The limit for the number of generations is selected to be 50; that is, we stop the iterations after the 50th generation. Therefore the number of trials to complete the optimization at a single frequency is about 1000–1500. A brute force approach to check all possible combinations of the five optimization variables with the same sampling would require $10^5$ trials, which is 100 times larger than that of GAs. For more populous LP

arrays leading to larger optimization spaces, the benefit gained from GAs becomes even more crucial compared to the brute force approach that has prohibitively high computational cost.

[24] Although GAs reduce the number of trials significantly compared to a brute force optimization, the calculation of the success for each individual has to be performed efficiently. We therefore employ the superposition technique as also sketched in Figure 4. For any LP array, the number of MLFMA solutions can be kept as low as the number of elements in the array. In each solution, we feed only one of the antennas with the excitation strength of unity. The vector current moment $\boldsymbol{F}(\theta, \phi)$ is then calculated and stored in the memory. We note that the solution by exciting one of the antennas in the array is different from the solution of a single antenna alone, since the former includes the mutual couplings between the antennas. Whenever it is required to test a set of values for the excitations, the vector current moments are multiplied by the corresponding coefficients and superposed to obtain a single vector current moment for the whole array. Then, we evaluate (7) and (17) to calculate the radiation intensity and the directive gain of the array, respectively.

[25] For the LP arrays considered in this paper, discretizations of the problems lead to matrix equations with 10,000–15,000 unknowns. Although the dimensions of these matrix equations are relatively small, MLFMA is still useful by providing significant acceleration compared to the direct solution. As an example, the direct solution of the radiation problem involving the three-element array in Figure 1a at a single frequency can be achieved in 50 minutes on a single processor of a 64-bit Intel Itanium server. Using MLFMA, this can be reduced to about 6 minutes, which becomes significant especially when the radiation problem is required to be solved at multiple frequencies. In this paper, we consider the solutions in the 300–800 MHz range sampled with 25 MHz intervals. Then, a total of $21 \times 3 = 63$ MLFMA solutions are performed for the three-element array, requiring about 6 hours. Using the solutions provided by MLFMA, optimizations are performed involving the operations of the GAs, superposition of the vector current moments, and the calculation of the directive gain. For the three-element array, optimizations at 21 frequencies can be achieved in one hour on a single processor of a 64-bit Intel Itanium server.

## 5. Results

[26] Finally, we present the results for the two circular-sectoral arrays depicted in Figure 1. Figures 5 and 6 show the far-field radiation patterns for the three-element and four-element arrays, respectively, demonstrating the beam-steering abilities of the arrays for 0°, 10°, 20°, 30°, 40°, and 50° on the azimuth plane. Since steering the beam at −10°, −20°, −30°, −40°, and −50° can also be realized by symmetry, a total scan range of 100° can be achieved. Optimization for $-\phi_0$ is easily obtained from the optimization for $+\phi_0$ by exchanging the order of the excitations among the antennas. Consequently, the width of the scannable sector becomes $2 \times 50° = 100°$ although the optimization is performed for the angles from 0° to 50°. In Figures 5 and 6, the directive gain is optimized in the $-x$ direction while rotating the arrays from 0° to 50° as depicted on the left of Figures 5 and 6.

[27] In Figures 5 and 6, the normalized radiation intensity is plotted in decibels (dB) for different frequencies from 400 MHz to 700 MHz. Because of the frequency independence, the radiation patterns do not change significantly in this range with respect to the frequency. When the array is rotated from 0° to 50°, the main beam is in the $-x$ direction because of the optimization by GAs. However, as the rotation angle is increased, it becomes difficult to keep the main beam in the $-x$ direction. Especially with the further increase of the rotation angle up to 60°–70° (not shown here), we observe that the main beam is not in the $-x$ direction anymore. In other words, although GAs attempt to maximize the directive gain in the $-x$ direction, the main beam cannot be pointed in the $-x$ direction.

[28] For more quantitative information, Figures 7a and 7b present the directive gain in the $-x$ direction as a function of the frequency with 25 MHz intervals and for different orientations of the three-element and four-element arrays, respectively. It can be observed that both of the arrays in Figures 5 and 6 provide directive gain over 9 in angular sectors of 100°. This is achieved in the frequency range from 300 MHz to 800 MHz and this range can be extended by adding more teeth to the LP antennas. On the other hand, Figure 7 also shows that the directive gain of the four-element array has larger fluctuations compared to the directive gain of the three-element array. This is due to the increasing mutual couplings among the antennas when the array becomes more populous. In other words, the mutual couplings among the antennas tend to deteriorate the frequency independence and this becomes more significant as the number of elements in the array is increased.

## 6. Concluding Remarks

[29] In this paper, we employ the recent advances in computational electromagnetics to properly design and simulate the circular-sectoral arrays of LP antennas, which can be useful in radar applications. Radiation characteristics of these arrays are investigated by emphasizing the frequency independence and the beam-steering ability. The excitations for the arrays of three and four LP antennas are optimized efficiently by GAs to

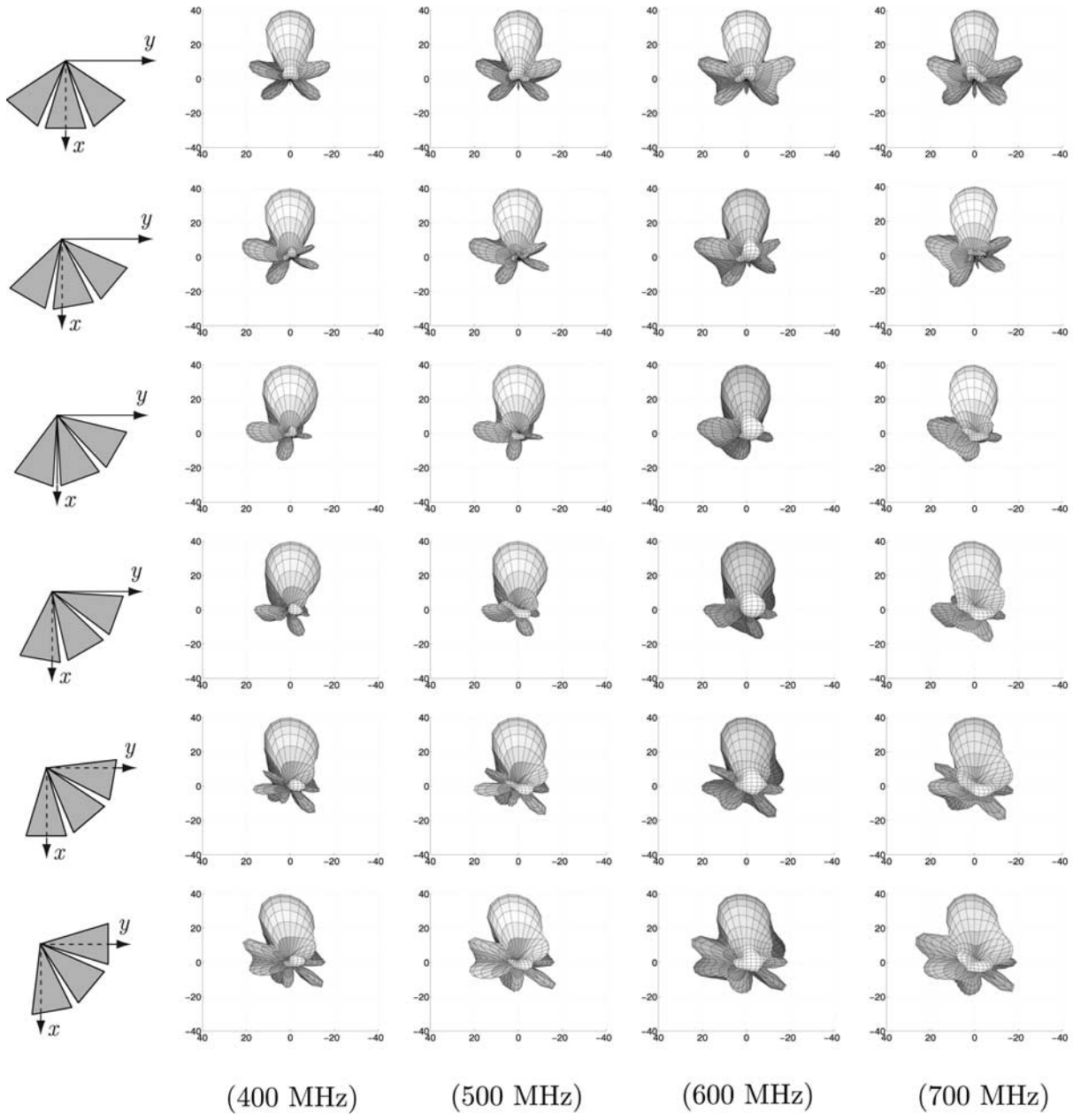


**Figure 5.** Normalized radiation intensity (in dB) of the array in Figure 1a for different frequencies and various rotated orientations as shown on the left. The directive gain is optimized in the $-x$ direction by the genetic algorithms.

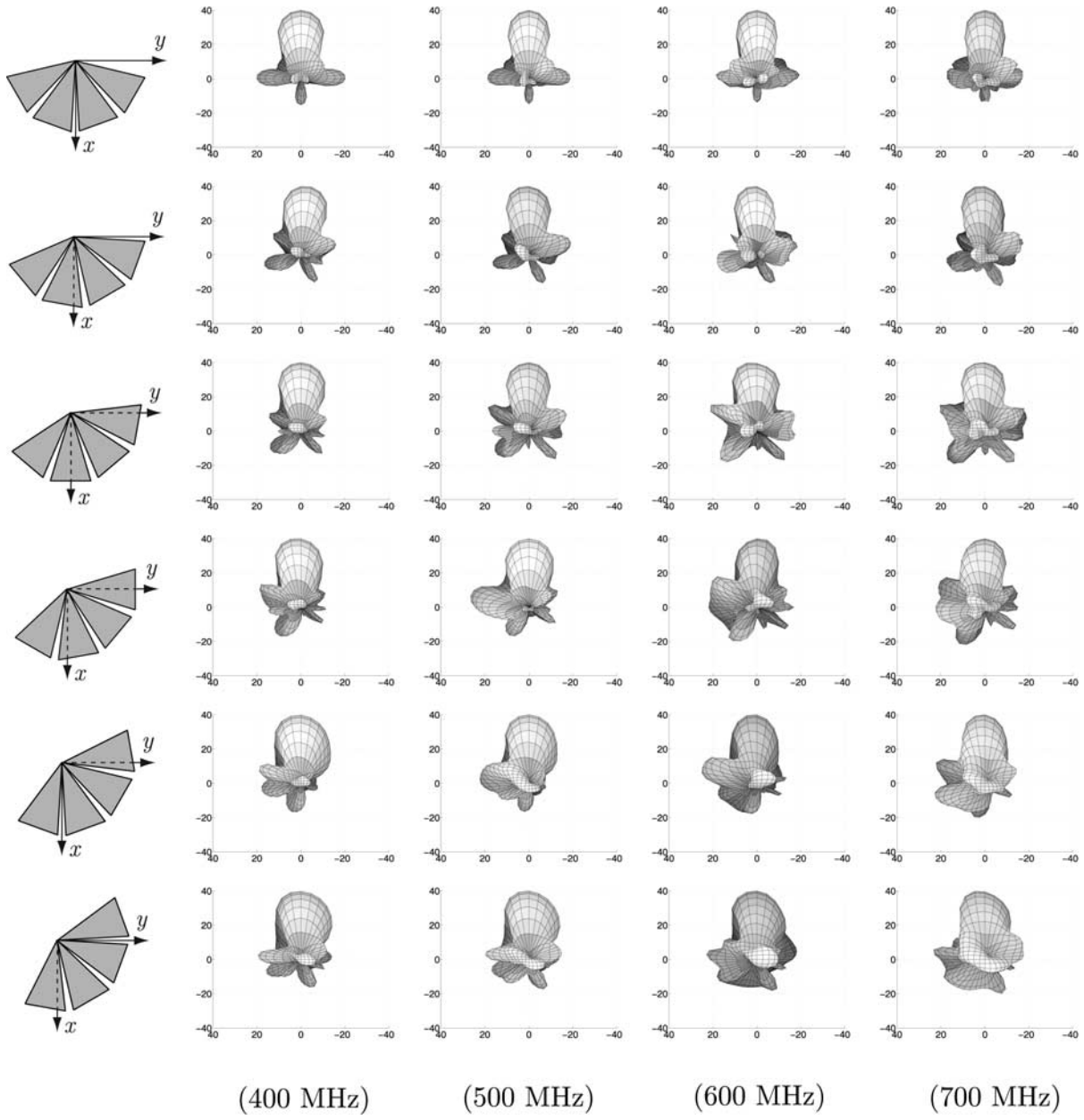


**Figure 6.** Normalized radiation intensity (in dB) of the array in Figure 1b for different frequencies and various rotated orientations as shown on the left. The directive gain is optimized in the $-x$ direction by the genetic algorithms.

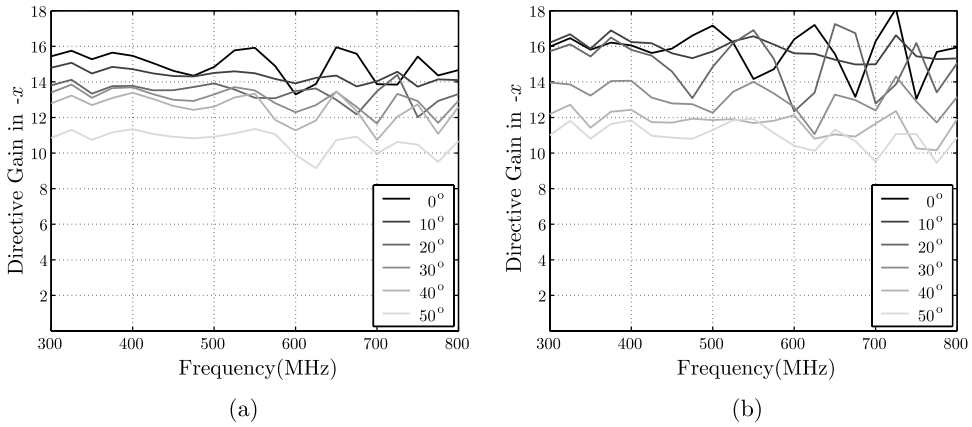


**Figure 7.** Directive gain in the $-x$ direction obtained by the genetic optimization for (a) the three-element array in Figure 1a and (b) the four-element array in Figure 1b. The arrays are rotated for different angles from 0° to 50° to test the beam-steering ability in a sector of 100°.

maintain the directive gain over 9 in the sectors up to 100°. Many other designs and configurations are possible to achieve an extended frequency range, an improved frequency independence, and a steering ability in other sectors.

[30] **Acknowledgments.** This work was supported by the Scientific and Technical Research Council of Turkey (TUBITAK) under Research Grant 105E172, by the Turkish Academy of Sciences in the framework of the Young Scientist Award Program (LG/TUBA-GEBIP/2002-1-12), and by contracts from ASELSAN and SSM.

## References

DuHamel, R. H., and D. E. Isbell (1957), Broadband logarithmically periodic antenna structures, *IRE Natl. Conv. Rec.*, *5*, 119–128.

DuHamel, R. H., and F. R. Ore (1958), Logarithmically periodic antenna designs, *IRE Natl. Conv. Rec.*, *6*, 139–152.

Eleftheriades, G. V., and J. R. Mosig (1996), On the network characterization of planar passive circuits using the method of moments, *IEEE Trans. Microwave Theory Tech.*, *44*, 438–445.

Ergül, Ö., and L. Gürel (2005), Nonplanar trapezoidal tooth log-periodic antennas: Design and electromagnetic modeling, *Radio Sci.*, *40*, RS5010, doi:10.1029/2004RS003215.

Ergül, Ö., and L. Gürel (2006), Design of circular log-periodic arrays using electromagnetic simulations, paper presented at IEEE Antennas and Propagation Society International Symposium 2006, Inst. of Electr. and Electron. Eng., Albuquerque, N. M.

Glisson, A. W., and D. R. Wilton (1980), Simple and efficient numerical methods for problems of electromagnetic radiation and scattering from surfaces, *IEEE Trans. Antennas Propag.*, *28*, 593–603.

Gürel, L., and Ö. Ergül (2005), Singularity of the magnetic-field integral equation and its extraction, *IEEE Antennas Wireless Propag. Lett.*, *4*, 229–232.

Kraus, J. D. (1988), *Antennas*, McGraw-Hill, Singapore.

Man, K. F., K. S. Tang, and S. Kwong (1999), *Genetic Algorithms: Concepts and Designs*, Springer, London.

Mayes, P. E. (1988), Frequency-independent antennas, in *Antenna Handbook: Theory, Applications, and Design*, edited by Y. T. Lo and S. W. Lee, Van Nostrand Reinhold, New York.

Rahmat-Samii, Y., and E. Michielssen (1999), *Electromagnetic Optimization by Genetic Algorithms*, John Wiley, New York.

Rao, S. M., D. R. Wilton, and A. W. Glisson (1982), Electromagnetic scattering by surfaces of arbitrary shape, *IEEE Trans. Antennas Propag.*, *30*, 409–418.

Rumsey, V. H. (1966), *Frequency Independent Antennas*, Academic, New York.

Song, J., C.-C. Lu, and W. C. Chew (1997), Multilevel fast multipole algorithm for electromagnetic scattering by large complex objects, *IEEE Trans. Antennas Propag.*, *45*, 1488–1493.

Stutzman, W. L., and G. A. Thiele (1981), *Antenna Theory and Design*, John Wiley, New York.

Ö. Ergül, Department of Electrical and Electronics Engineering, Bilkent University, TR-06800, Bilkent, Ankara, Turkey. (ergul@ee.bilkent.edu.tr)

L. Gürel, Computational Electromagnetics Research Center, Bilkent University, TR-06800, Bilkent, Ankara, Turkey. (lgurel@bilkent.edu.tr)